Article

Atomically Dispersed Ru on Manganese Oxide Catalyst Boosts Oxidative Cyanation

Hai Wang, Dongyang Xu, Erjia Guan, Liang Wang, Jian Zhang, Chengtao Wang, Sai Wang, Hua Xu, Xiangju Meng, Bo Yang, Bruce C. Gates, and Feng-Shou Xiao

ACS Catal., **Just Accepted Manuscript** • DOI: 10.1021/acscatal.0c00485 • Publication Date (Web): 07 May 2020

Atomically Dispersed Ru on Manganese Oxide Catalyst Boosts Oxidative Cyanation

Hai Wang[a,#], Dongyang Xu[b,#], Erjia Guan[c,#], Liang Wang[a,], Jian Zhang[e], Chengtao Wang[d], Sai Wang[d], Hua Xu[d], Xiangju Meng[d], Bo Yang[b,*], Bruce C. Gates[c], and Feng-Shou Xiao[a,d,e,*]*

[a]Key Lab of Biomass Chemical Engineering of Ministry of Education, College of Chemical and Biological Engineering, Zhejiang University, Hangzhou 310027, China.

[b]School of Physical Science and Technology, ShanghaiTech University, Shanghai 201210, China.

[c]Department of Chemical Engineering, University of California, Davis CA 95616, United States.

[d]Key Lab of Applied Chemistry of Zhejiang Province, Department of Chemistry, Zhejiang University, Hangzhou 310028, China.

[e]Beijing Advanced Innovation Center for Soft Matter, Science and Engineering, Beijing University of Chemical Technology, Beijing 100029, China.

[*]Corresponding author: liangwang@zju.edu.cn; yangbo1@shanghaitech.edu.cn; fsxiao@zju.edu.cn

[#] H. Wang, D. Xu, and E. Guan contributed equally.

ABSTRACT

There is a strong incentive for environmentally benign and sustainable production of organic nitriles to avoid the use of toxic cyanides. Here we report that manganese oxide nanorod-supported single-site Ru catalysts are active, selective, and stable for oxidative cyanation of various alcohols to give the corresponding nitriles with molecular oxygen and ammonia as the reactants. The very low amount of Ru (0.1 wt%) with atomic dispersion boosts the catalytic performance of manganese oxides. Experimental and theoretical results show how the Ru sites enhance the ammonia resistance of the catalyst, bolstering its performance in alcohol dehydrogenation and oxygen activation, the key steps in the oxidative cyanation. This investigation demonstrates the high efficiency of a single-site Ru catalyst for nitrile production.

Keywords: single-site Ru; nanorod manganese oxide; oxidative cyanation; ammonia; nitrile

1. INTRODUCTION

Organic nitriles play essential roles in chemical technology, in applications for producing pharmaceuticals, agrochemicals, fine chemicals, and building blocks for high-performance polymers, rubbers, and molecular electronics.[1-6] The classical routes for production of organic nitriles employ toxic HCN or metal cyanides (e.g., KCN, NaCN, and CuCN),[5] and these are associated with the tragic environmental disasters at Bhopal in 1984 and Baia Mare, Romania, in 2000. There is a need for sustainable technology to avoid these toxic chemicals.

Several routes have been developed for nitrile synthesis without cyanides, including, for example, the hydroxylamine route using a clay catalyst, whereby the hydroxylamine hydrochloride reactant was used under microwave conditions.[7] Catalytic ammoxidation has emerged as a preferred route nitrile synthesis, with molecular ammonia being used as the nitrogen source reacting with hydrocarbons,[3] alcohols,[2,4,8] or aldehydes[8]. The ammoxidation processes generally takes place with solid catalysts and gaseous reactants at high temperatures (300–550 °C), being limited by over-oxidation to form CO_2 and thus insufficient selectivities to nitriles.[5,9] Moreover, the strongly corrosive nature of gaseous ammonia at high temperatures is a serious issue. Liquid-phase ammoxidation can be carried out to effectively hinder the over-oxidation under mild reaction reactions, with high activities offered by copper complex catalysts.[10,11] However, these processes are limited by the catalyst separation and regeneration challenges that are intrinsic to homogeneous catalysis. Seeking improved

solid catalysts, researchers have reported successes with $Ru(OH)_3$,[8] ferric and cobalt carbides,[2,12] Au-[13] and Pt-containing catalysts,[14] and manganese oxide.[4,15,16] However, correlations between catalyst structure and performance are still lacking, and we posit that new insights would help to accelerate the development of new catalysts with enhanced performance for oxidative cyanations.

Now we report a manganese oxide-supported catalyst that is highly efficient for the oxidative cyanation. Key to the success of this catalyst is atomically dispersed ruthenium on the support, used in the form of nanorods (denoted as MnO_2-*r*). The catalyst, *x*Ru/MnO_2-*r* (*x* is the Ru loading in wt percent), was made by a wet-chemical method with Ru loadings as low as 0.1 wt%. The data presented herein show that the single-site Ru remarkably boosts the catalytic activity for oxidative cyanation of aliphatic, benzylic, allylic, and heterocyclic alcohols into the corresponding nitriles by enhancing the ammonia resistance of the catalyst and accelerating the alcohol dehydrogenation and oxygen activation. These are new characteristics of atomically dispersed (single-site) catalysts.

2. EXPERIMENAL SECTION

2.1. Catalyst Preparation. *Synthesis of nanorod α-MnO_2 (MnO_2-r).* In a typical synthesis, an aqueous solution of $KMnO_4$ (0.37 *M*, 50 mL) was added dropwise into a stirred aqueous solution of $MnSO_4$ (1.73 *M*, 15 mL). After stirring at room temperature for another 0.5 h, the resultant precipitate was collected by filtration, washed with a

large excess of deionized water, and dried at 150 °C overnight to give the MnO_2-*r* sample.

Synthesis of Ru/MnO_2-r. $RuCl_3$ (2.1 mg) was dissolved in 85 mL of deionized water, followed by addition of 10 mL of aqueous NaOH (0.2 *M*) solution with stirring. Then 1.0 g of as-synthesized MnO_2-*r* was added and the mixture stirred at 50 °C for 12 h. The slurry was separated by centrifugation, and the resultant solid was washed with an excess of deionized water, then dried at 150 °C for 2 h to give the Ru-loaded sample. Analysis of the product by ICP-OES determined a Ru loading of 0.1 wt%, with the sample denoted 0.1Ru/MnO_2-*r*. Ru/MnO_2-*r* catalysts with different Ru contents were synthesized similarly but with different masses of $RuCl_3$ in the starting solution: 0.20, 6.16, and 63.47 mg of $RuCl_3$ for the synthesis of 0.01Ru/MnO_2-*r*, 0.3Ru/MnO_2-*r*, and 3.0Ru/MnO_2-*r*, respectively.

Synthesis of Pd/MnO_2-r, Pt/MnO_2-r, Rh/MnO_2-r, Au/MnO_2-r, Ag/MnO_2-r, and Fe/MnO_2-r. These catalysts were prepared by prodecures similar to that stated above for the synthesis of Ru/MnO_2-*r*, except that Na_2PdCl_4 (6.0 mg_{Pd} mL^{-1}, 0.5 mL), H_2PtCl_6 (7.50 mg_{Pt} mL^{-1}, 0.40 mL), $RhCl_3$ (7.92 mg_{Rh} mL^{-1}, 0.38 mL), $HAuCl_4$ (9.56 mg_{Au} mL^{-1}, 0.32 mL) aqueous solutions and solid $AgNO_3$ (5.00 mg), $FeCl_3 \cdot 6H_2O$ (15.0 mg) were used as precursors, respectively. The Pd, Pt, Rh, Au, Ag, and Fe loadings were controlled to be ~0.3 wt% for these samples.

Synthesis of Ru/CeO_2, Ru/MnO, Ru/A-MnO_2, Ru/Mn_2O_3, Ru/Mn_3O_4, Ru/Co_3O_4, Ru/SiO_2, Ru/C, and Ru/Al_2O_3. In a typical synthesis, of Ru/CeO_2, 2.1 mg of $RuCl_3$ was

dissolved in 85 mL of deionized water with stirring, followed by the addition of an aqueous NaOH solution (0.2 *M*, 10 mL). Then 1.0 g of CeO_2 was added and the mixture stirred at 50 °C for another 12 h; the resultant solid product in the slurry was separated by centrifugation, washed with deionized water, and dried at 150 °C for 2 h, giving the Ru/CeO_2 sample with a Ru loading of 0.1 wt%. The Ru/MnO, $Ru/A\text{-}MnO_2$, Ru/Mn_2O_3, Ru/Mn_3O_4, Ru/Co_3O_4, Ru/SiO_2, Ru/C, and Ru/Al_2O_3 catalysts were synthesized similarly, but with the supports being MnO, $A\text{-}MnO_2$, Mn_2O_3, Mn_3O_4, Co_3O_4, SiO_2, carbon, and Al_2O_3, respectively.

2.2. Characterization of Catalysts. X-ray diffraction (XRD) patterns were obtained with a Rigaku D/MAX 2550 diffractometer with Cu Kα radiation (λ = 1.5418 Å). Metal loadings were determined by inductively coupled plasma optical emission spectrometry (ICP-OES) analysis (Perkin-Elmer 3300DV). Transmission electron microscopy (TEM), scanning transmission electron microscopy (STEM), and energy dispersive spectroscopy were carried out with a Cs-corrected JEM-ARM300F electron microscope (JEOL, Japan) with an acceleration voltage of 300 kV. EXAFS data at the ruthenium K-edge were recorded at beamline 8-ID at NSLS-II. In these experiments, each sample (approximately 50 mg) was pressed into a wafer and sealed with Kapton tape. Each sample was tested in air at room temperature. The spectra were collected in fluorescence mode, and at least 10 scans were collected for each sample to optimize data quality. Analysis of the EXAFS data was carried out with the software ATHENA and ARTEMIS of the IFEFFIT package.[17] Theoretical phases and amplitudes of single scattering paths were obtained in FEFF for a ruthenium oxide reference,[18] and a

theoretical model was built with single-site Ru located on Mn defect sites in MnO_2.

2.3. Catalyst Performance Evaluation. *Oxidative Cyanation of Alcohols.* Oxidative cyanation reactions were carried out in a high-pressure steel autoclave reactor equipped with a PTFE bottle, magnetic stirrer (900 rpm), and an explosion-proof pressure sensor. In a typical run, the as-synthesized catalyst, aqueous ammonia (28–30% NH_3), and substrate alcohols were dispersed within *t*-amyl alcohol solvent in the reactor, and then the autoclave was purged with oxygen for three times. Then the reactor, equipped with an internal thermocouple, was quickly heated to the desired temperature and controlled at that temperature (the reaction temperature was measured by a thermocouple in the autoclave), and the autogenous pressure was measured and maintained. After the desired reaction time, the reactor was placed in an ice bath to quench the reaction. After separation of the solid catalyst, the liquid products and unconverted reactants were analyzed with a Shimadzu GC-2014 gas chromatograph equipped with a flame ionization detector (FID) and an Agilent HP-6890 gas chromatograph-mass spectrometer, with bromobenzene and hexadecane used as internal standards. The products with high boiling points were analyzed by ^{13}C and ^{1}H NMR spectroscopies. The gas-phase products (e.g., CO and CO_2) were analyzed with a Fu Li-9790 gas chromatograph equipped with a thermal conductivity detector (TCD). (Safety Note: The high-pressure oxygen or air are widely used in the aerobic oxidations,[19,20] and the reaction systems in this work were out of the explosion limits of the reactants. For example, the explosion limit of benzyl alcohol is 1.3-13.0% in oxygen, and the concentration of benzyl alcohol in the gaseous phase in the reactor is in a 0-0.4% region.

The same trends also occur for *n*-heptanol. Furthermore, the fire and static electricity are still not allowed to access the internal reactor for safety reasons.

Catalytic Dehydrogenation of Methanol. The dehydrogenation of methanol was carried out in a continuous-flow vertical fixed-bed glass reactor with length of 0.5 m and an internal diameter of 6 mm. Methanol was injected into the reactor with a pump, and the flow rate of NH_3 was controlled with a mass flow controller. Typically, 100 mg of catalyst particles (40-60 mesh) mixed with 300 mg of quartz sand (40-60 mesh) were localized within the reactor tube, with the flow rate of the 1.0 volume% NH_3 in N_2 being 10 sccm; the injection rate of the methanol was 1.2 mL/h, and the reaction temperature was 300 °C. The gas-phase products were analyzed on-line with a Fu Li-9790 gas chromatograph equipped with a TCD.

Recycling Test and Hot Filtration Experiment. After each reaction experiment, the catalyst was removed from the reactor and washed with ethanol/deionized water, dried overnight at 150 °C, and then used in the next experiment to evaluate its recyclability. Hot filtration was carried out to evaluate the catalyst leaching in the reaction liquor. After oxidative cyanation of *n*-heptanol for 4 h (0.2 mmol of *n*-heptanol, 100 mg of 0.1Ru/MnO_2-*r*, 4 mL of *t*-amyl alcohol solvent, 100 μL of aqueous NH_3 (28-30% NH_3), 2.0 MPa of oxygen, 100 °C), the gas produced in the reaction was released after cooling of the reactor to room temperature. Then the resultant product mixture was filtered at 80 °C, and a known mass of *t*-amyl alcohol solvent and another 100 μL of aqueous ammonia were added to the liquor to make the total volume 4 mL, which was then used

in the next experiment without additional catalyst.

Analysis of Catalyst Performance Data. The conversion, product yields, and selectivity in the oxidative cyanation were calculated according to the following equations:

$$\text{Conversion} = \left(\frac{\text{Moles of substrate converted}}{\text{Moles of substrate fed}}\right) \times 100\%$$

$$\text{Yield of product} = \left(\frac{\text{Moles of product}}{\text{Moles of substrate fed}}\right) \times 100\%$$

$$\text{Selectivity to product} = \left(\frac{\text{Moles of product}}{\text{Moles of substrate converted}}\right) \times 100\%$$

In the kinetics study, the average reaction rates were calculated from the moles of substrate converted per gram of catalyst in one hour (mmol g_{cat}^{-1} h^{-1}), with the conversion of substrate controlled to be lower than 20.0%.

Carbon balances. The carbon balances before and after reaction were based on the number of carbon atoms in all the reactants and products in the liquor before and after reaction. The CO_2 formed by over-oxidation was not included in calculating the carbon balances. The carbon balance values were calculated according to the following equation:

$$C\% = \frac{M_f * 7 + M_1 * n_1 + M_2 * n_2 + M_3 * n_3 + \ldots + M_x * n_x}{M_e * 7} \times 100\%$$

Here C% is the carbon balance closure percentage, M_f is the final number of moles of *n*-heptanol in the reactor after reaction; 7 is the number of carbon atoms in a single *n*-

heptanol molecule; M_1 (M_2, M_3, … M_x) are the numbers of moles of liquid product 1 (product 2, 3,……x) in the reactor after reaction; n_1 (n_2, n_3,…..n_x) is the number of carbon atoms in a single molecule of product 1 (product 2, 3,……x); M_e is the moles of *n*-heptanol in the feed before reaction.

2.4. Computational Details. All the density functional theory (DFT) calculations were performed with the VASP package[21] using the PBE functional and the projector augmented wave (PAW) pseudopotential.[22] The van der Waals interactions were described with Grimme's empirical three-body dispersion correction in the scheme of Becke-Johnson damping, namely, PBE-D3(BJ).[23] Hubbard *U* corrections were used, and we employed $U - J = 5.2$ eV, for the spherical part of the interaction, and $J = 1.0$ eV, according to the values reported.[24] The calculated lattice parameters for α-MnO_2 with the PBE + U approach were a = b = 9.814 Å and c = 2.895 Å, which agree well with the experimental parameters (a = b = 9.750 Å and c = 2.861 Å).[25] The (100) surface dominates and represents 54% of the *α*-MnO_2 surface area with low energies of 0.64 J m^{-2} according to a previous report.[24] This present work built the optimized MnO_2 (100) slab with a dimension of 9.81 × 8.69 × 23 Å, consisting of 48 O and 24 Mn atoms. The bottom halves of the slabs were frozen at their bulk positions, and the rest of the atoms were relaxed. A value of the cut-off energy of 400 eV and a *k*-point mesh of 3 × 3 × 1 were employed. For Al_2O_3, a plane-wave basis set with a cutoff energy of 400 eV and a 6 × 6 × 2 *k*-point grid generated with the Monkhorst−Pack scheme were found to give converged results. A surface slab consisted of 48 O atoms and 32 Al atoms, and the slabs were separated by a vacuum with a spacing of 15 Å in the z-direction to stabilize

the species in the slabs. The dimensions of the $Al_2O_3(0001)$ surface slab used in the calculations were: a = 8.253 Å, b = 9.530 Å, and c = 20.660 Å.

3. RESULTS AND DISCUSSION

3.1. Evaluation of Data Characterizing *n*-Heptanol Cyanation.

Figure 1 shows data characterizing the catalytic performance in a challenging reaction: oxidative cyanation of *n*-heptanol. The data provide a comparison of the performance of the supported catalyst containing 0.3 wt% Ru with that of the support MnO_2-*r* alone, which itself is highly active (*n*-heptanol conversion of 40.7% with 94.3% selectivity to heptanonitrile under our conditions) (Table S1, Entry 2). Addition of Ru to the support led to marked increases in both the *n*-heptanol conversion and heptanonitrile selectivity, illustrated, for example, by the conversion of 66.9% with >99.5% selectivity to heptanonitrile under these conditions (Figure 1, Table S1). Even with a decreased Ru loading of 0.1 wt%, the catalyst gave an *n*-heptanol conversion of 58.3% with unchanged selectivity. Increasing the reaction time from 2 to 5 h led to an improved *n*-heptanol conversion of 82.4% with a nitrile selectivity of 98.3%.

When metals other than Ru were incorporated in the catalyst (Au, Pt, Pd, Rh, Ag, or Fe), however, the conversion and selectivity in the *n*-heptanol oxidative cyanation were markedly less, than with the MnO_2-*r* catalyst (Figure 1, Table S1), which might

be an indication that these additives blocked part of the MnO_2-*r* surface sites. These results indicate that the Ru sites play a critical role in the *n*-heptanol oxidative cyanation.

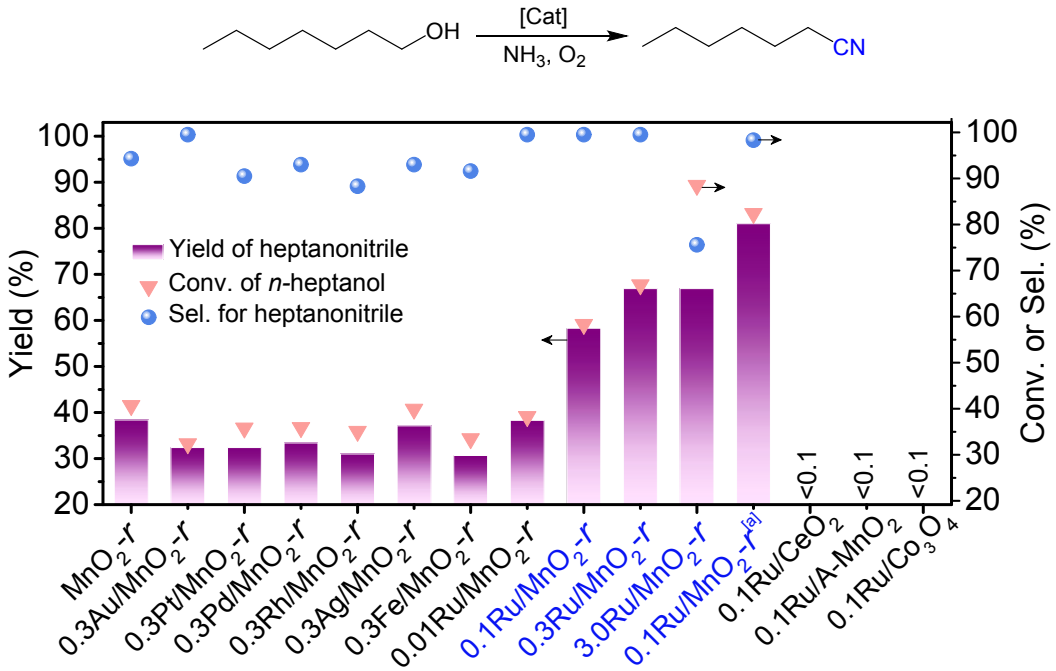

Figure 1. Performance data characterizing oxidative cyanation of *n*-heptanol with various catalysts. Reaction conditions: 0.2 mmol of substrate, 4 mL of *t*-amyl alcohol, 100 μL of aqueous NH_3 (28–30 wt%), 100 mg of catalyst, 2.0 MPa of oxygen, 100 °C, 2 h. [a]Reaction time: 5 h. The carbon balance data are shown in Table S1 in the Supporting Information.

It is well known that $Ru(OH)_3$ present at a high loading (>2.0 wt%) on a support is active for the oxidative cyanation,[8] but Ru at a low loading (0.1 wt%) on the supports CeO_2, commercial activated MnO_2 (A-MnO_2), Co_3O_4, MnO, Mn_3O_4, and Mn_2O_3 does not catalyze this oxidative cyanation (Figures 1, S1, and S2, Tables S2 and S3 in the Supporting Information)-with the exception of MnO_2-*r*. These results demonstrate that both the Ru and MnO_2-*r* are necessary for the catalysis. Increasing the loading of Ru (to 3.0 wt%) increased the activity for the *n*-heptanol transformation, but at the cost of lower heptanonitrile selectivity, as more CO_x formed by over-oxidation (Figure 1, Table

S1 in the Supporting Information).

3.2. Investigation of a Range of Substrates. Figure 2 includes data characterizing the synthesis of a group of substituted and functionalized benzonitriles in the presence of the 0.1Ru/MnO_2-*r* catalyst. These substrates include aliphatic, allylic, alkynyl, and other, structurally diverse, heterocyclic nitriles. Under mild reaction conditions (0.5 MPa of oxygen, 100 °C, 0.025 mol% of Ru with an S/C ratio of ~4042, where this is the molar ratio of substrate to Ru in the reaction system), the functionalized benzylic nitriles with electron-donating or electron-withdrawing substituents were efficiently synthesized with high yields (Figure 2, **1-17**). In particular, the halogenated benzonitriles, which can be used for the preparation of dyes, pharmaceuticals, potential high-performance pesticides, and specialty engineering plastics, were also synthesized with yields exceeding 71.7%, giving the corresponding by-product amides from the side-reaction nitrile hydration. Considering that the amides are also a class of valuable product and could be transformed into nitriles by simple dehydration,[26] we also include them in the evaluation of the product yields characterizing the various substrates (the total yields of nitriles and amides are given in parentheses in Figure 2) that gave greater than 99.0% yields of nitriles and amides for these substrates (Figure 2, **1-17**). The sterically hindered substrate, such as 2-methoxybenzyl alcohol, were also successfully transformed into the corresponding nitriles with yields >99.0% (Figures 2, **9**). Significantly, the relatively complex substrates, such as quinoline-6-carbonitrile, piperonyl alcohol, biphenyl-4-methanol, 4-phenoxyphenyl methanol, 4-benzyloxybenzyl alcohol, and 3,5-dibenzyloxybenzyl alcohol, were also selectively

converted into the corresponding nitriles in >90% yields (Figure 2, **18-23**).

Compared with the benzylic alcohols, aliphatic alcohols usually have lower reactivities.[2,13] Nonetheless, the 0.1Ru/MnO_2-*r* catalyst still exhibited high efficacy for the ammoxidation of aliphatic alcohols under our reaction conditions (0.5 MPa of oxygen, 100 °C, S/C at ~1010). For example, the alcohols 1-hexanol, *n*-heptanol, 1-nonanol, 1-decanol, and 4-phenylbutan-1-ol were almost fully transformed on 0.1Ru/MnO_2-*r* (Figure 2, **24-28**), giving >90% yields to the desired nitriles and amides.

In the transformation of allylic and alkynyl alcohols, the side reactions of isomerization, hydration, and over oxidation usually occur.[8] But the 0.1Ru/MnO_2-*r* catalyst still gave nitrile yields higher than 99.0% from the substrates cinnamyl alcohol, geraniol, and 4-ethynylphenyl methanol (Figure 2, **29-31**). In particular, the structurally complex 3,7-dimethyl-2,6-octadienenitrile was effectively synthesized with a yield >99.0%, showing that the catalyst clearly outperformed Cu[11] and Co/Fe catalysts,[2] which have been reported to be highly efficient. Furthermore, in the oxidative cyanations of heterocyclic alcohols including 3-pyridinemethanol, furfuryl alcohol, and 3-thiophenemethanol, the 0.1Ru/MnO_2-*r* catalyst still gave >99% yields to the nitriles (Figure 2, **32-34**). Such performances are even comparable with those in the conventional heterocyclic nitrile synthesis route *via* the cyanation of heteroaryl halide.[5]

a General reaction scheme

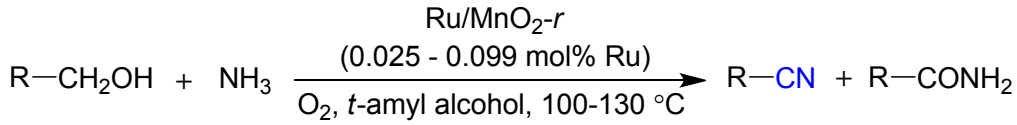

b Substituted and functionalized benzonitriles

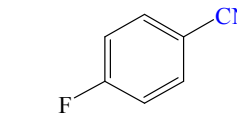

1: >99.0% 5h

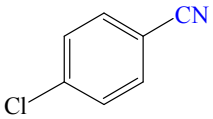

2: >99.0% 5h

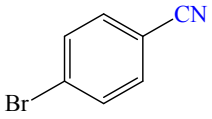

3: >99.0% 4h

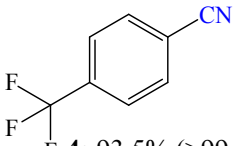

4: 93.5% (>99.0) 4h

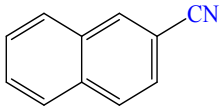

5: >99.0% 4h

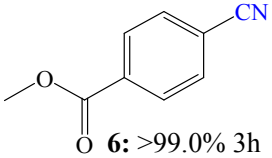

6: >99.0% 3h

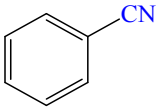

7: >99.0% 5h

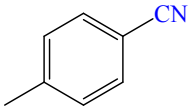

8: >99.0% 7h

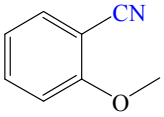

9: >99.0% 12h

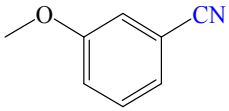

10: >99.0% 10h

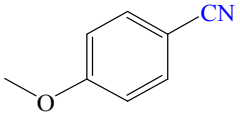

11: >99.0% 8h

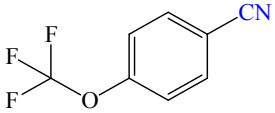

12: 95.5% (>99.0) 4h

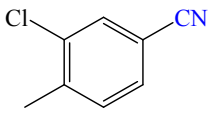

13: 86.4% (>99.0) 1.5h‡

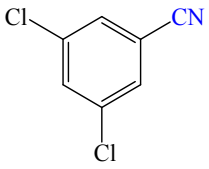

14: 71.7% (>99.0) 3h

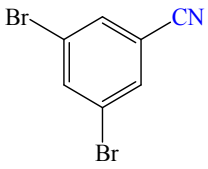

15: 77.3% (>99.0) 5.5h

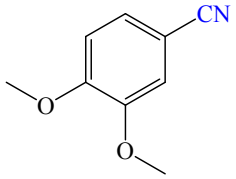

16: >99.0% 12h

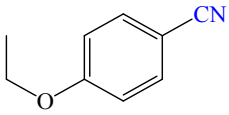

17: >99.0% 12h

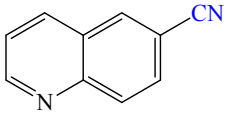

18: >99.0% 4h

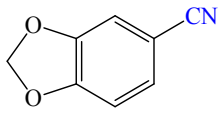

19: >99.0% 4h

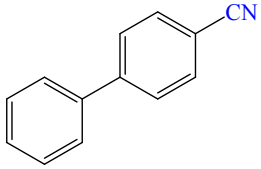

20: >99.0% 6h

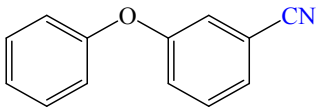

21: 98.3% 10h

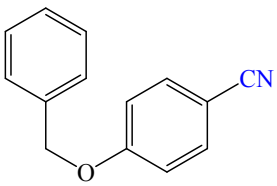

22: >99.0% 14h

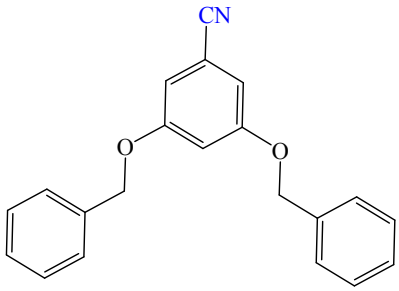

23: 90.0% (>99.0%) 14h

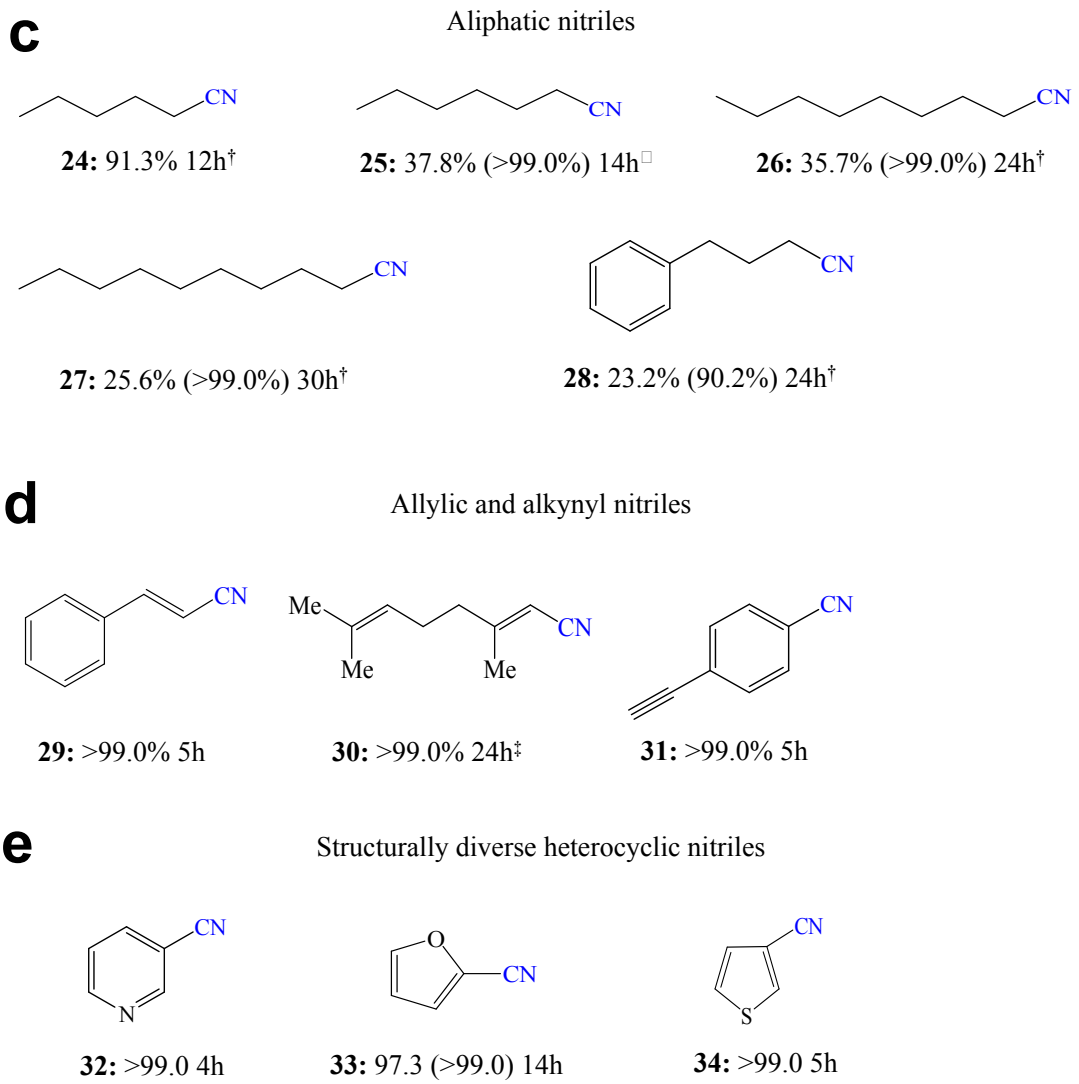

Figure 2. Synthesis of different types of nitriles catalyzed by 0.1Ru/MnO_2-*r*. Reaction conditions: 0.4 mmol of substrate, 4 mL of *t*-amyl alcohol, 100 μL of aqueous NH_3 (28–30 wt%), 10 mg of catalyst (0.025 mol% Ru), 0.5 MPa of oxygen, 100 °C. The values in parentheses are yields of the nitriles and amides. □20 mg of catalyst (0.05 mol% Ru). †0.2 mmol of substrate, 200 μL of aqueous NH_3 (28–30 wt%), 20 mg of catalyst (0.099 mol% Ru), 120 °C. □0.2 mmol of substrate, 200 μL of aqueous NH_3 (28–30 wt%), 20 mg of catalyst (0.099 mol% Ru), 130 °C. ‡30 mg of catalyst (0.074 mol% Ru).

Moreover, the catalyst 0.1Ru/MnO_2-*r* was used in the gram-scale synthesis of

various nitriles, and high yields were still obtained (Figure 3)—results that might suggest the potential practicability of the 0.1Ru/MnO_2-*r* catalyst. These data confirm the catalytic performances of 0.1Ru/MnO_2-*r* catalyst in the oxidative cyanation of various substrates (Tables S4 and S5 in the Supporting Information).

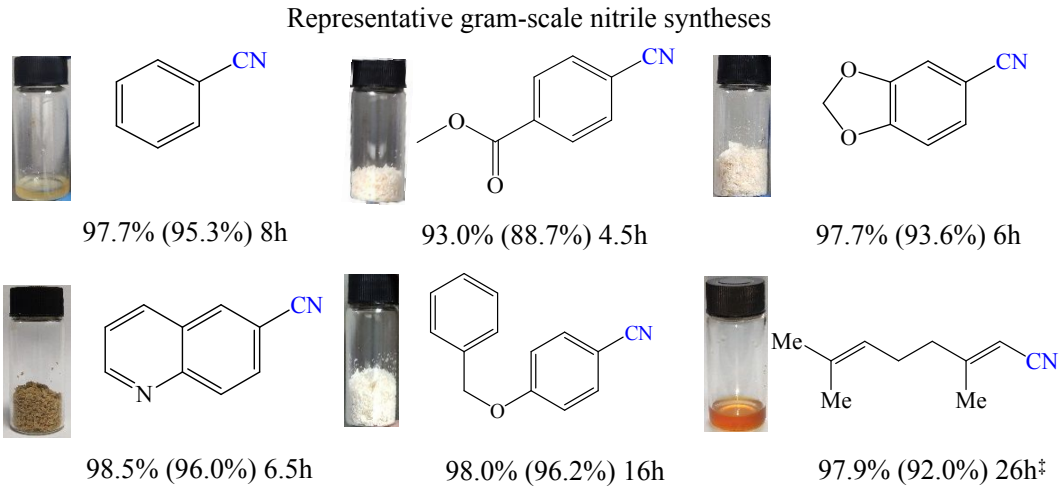

Figure 3. Gram-scale syntheses of nitriles catalyzed by 0.1Ru/MnO_2-*r*. Reaction conditions: 1 g of substrate, 60 mL of *t*-amyl alcohol, 100 μL of aqueous NH_3 (28–30 wt%) for each 0.4 mmol substrate, 0.1Ru/MnO_2-*r* (0.025 mol% Ru), 0.5 MPa of oxygen, 100 °C. ‡0.074 mol% Ru. The values in parentheses are the yields of isolated products. The photographs show the products isolated from the reaction system.

3.3. Catalyst Recyclability. We further emphasize that the 0.1Ru/MnO_2-*r* catalyst is stable in the reaction solution, as confirmed by the results of a hot filtration experiment (Figure S3 in the Supporting Information). After each reaction run, the catalyst was easily separated from the products, washed with ethanol and water, dried, and reused. In the continuous recycling tests (Figure S4 in the Supporting Information), the catalyst 0.1Ru/MnO_2-*r* exhibited stable performance with undetectable deactivation. Moreover, we did not observe Ru leaching by characterization of the post-reaction solutions by ICP analyses, a further indication of the excellent recyclability of the catalyst.

3.4. Catalyst Structure Characterization. To indentify the catalyst structure and function of Ru species, multiple characterizations, catalyst performance measurements, and computational simulations were performed. Figure S5 in the Supporting Information shows XRD patterns of MnO_2-*r* and 0.1Ru/MnO_2-*r*, including weak, broad peaks associated with α-MnO_2 crystals (Figure S6 in the Supporting Information). In contrast, XRD patterns indicative of metallic Ru, RuO_x, or $Ru(OH)_3$ species were undetectable, pointing to a high dispersion of the Ru species on the support.

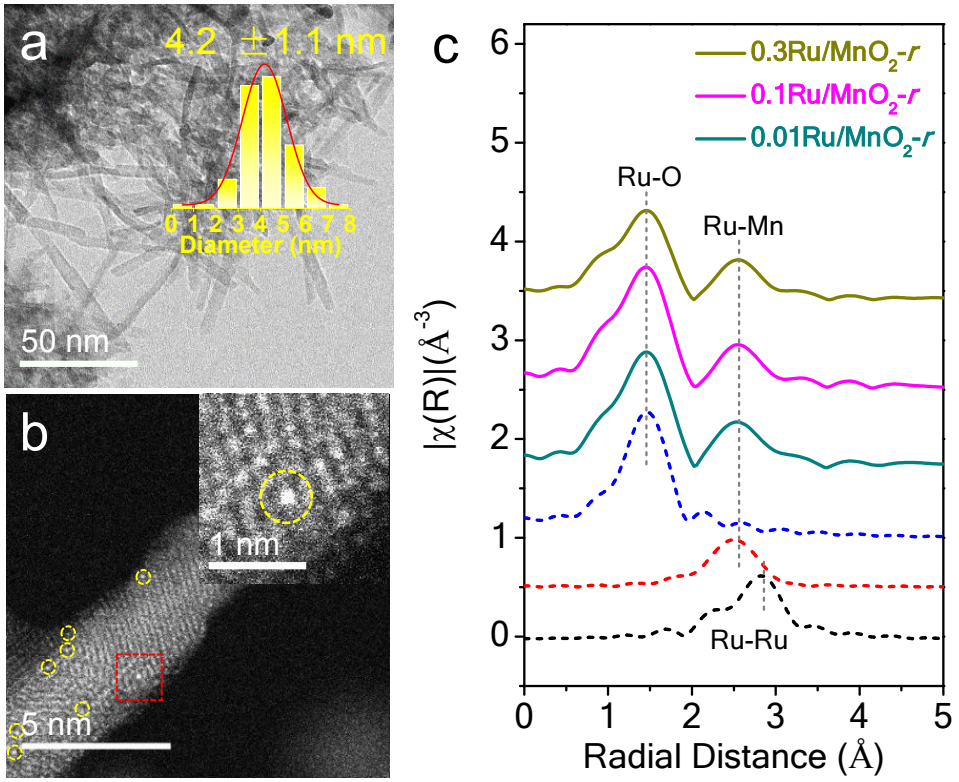

Figure 4. (a) TEM and (b) high-resolution HAADF-STEM images of the catalyst 0.1Ru/MnO_2-*r*. Inset in (a), distribution of diameters of the nanorods; inset in (b), enlarged view of the area in the red square in the HAADF-STEM image. The atomically dispersed Ru is highlighted by yellow circles. (c) Ru *K*-edge EXAFS spectra in *R*-space of various catalysts. The dotted lines are as follows: black, Ru-Ru and blue, Ru-O single scattering paths generated from a Ru oxide reference, and red, Ru-Mn single scattering

path generated with *FEFF* models of single-site Ru dispersed on MnO_2.

Transmission electron microscopic images of the 0.1Ru/MnO_2-*r* show a nanorod morphology, with small diameters, 3–5 nm (Figure 4a, inset, Figure S7 in the Supporting Information). Aberration-corrected high-angle annular dark-field scanning transmission electron microscopy (HAADF-STEM) provided direct atomic-resolution observations of the Ru atoms (Figure 4b). The elemental distributions of Mn and O are shown by energy dispersive X-ray data (EDX), but the signal of Ru is much weaker, consistent with its low loading and high dispersion (Figures S8 and S9 in the Supporting Information). Significantly, there is no evidence of Ru nanoparticles/nanoclusters in the HAADF-STEM images—evidently, all of the ruthenium was atomically dispersed. Not only do the STEM images of the 0.1Ru/MnO_2-*r* sample provide no evidence of Ru nanoclusters/nanoparticles, they demonstrate that the isolated Ru atoms occupy exactly the positions of missing Mn atoms at the support surface (inset, Figure 4b), in good agreement with earlier reports showing the presence of catalytic metals at support surface sites.[27,28]

Further characterization by extended X-ray absorption fine structure (EXAFS) spectroscopy showed Ru–O (distance R = 1.48 Å, before phase correction) and Ru–Mn (R = 2.58 Å, before phase correction) contributions characterizing 0.01Ru/MnO_2-*r*, 0.1Ru/MnO_2-*r*, 0.3Ru/MnO_2-*r*, and 3.0Ru/MnO_2-*r* samples, consistent with the bonding of the isolated Ru atoms to MnO_2-*r via* Ru–O bonds (Figure 4c, Figure S10 in the Supporting Information). These data gave no evidence of edge features characteristic of metallic Ru or Ru–O–Ru, in agreement with the atomic Ru dispersion.

The XPS data characterizing the 0.1Ru/MnO_2-*r* catalyst give evidence of the Ru $3p_{3/2}$ binding energy at 464.4 eV (Figure S11a in the Supporting Information), which has a significant shift to higher energy compared with metallic Ru^0 and is assigned to positively charged Ru.[29,30] Such feature is associated with the interaction between a single-site Ru and the MnO_2-*r* matrix *via* an Ru–O–Mn linkage involving interfacial oxygen species (Figure S11b in the Supporting Information), in good agreement with many observations characterizing metal oxide-supported single-site species.[28,31,32]

X-ray absorption near-edge structure (XANES) spectra of Ru/ MnO_2-*r* catalysts (Figure S11c in the Supporting Information) show the Ru *K*-edge white lines with higher energy and stronger intensities than in the spectra of Ru foil. This result confirms the positive oxidation state of Ru in the sample,[29,33,34] consistent with the XPS results.

3.5. Reaction Pathways and Kinetics. To better understand the role of the single-site Ru on MnO_2-*r* as a catalyst, we did further experiments characterizing oxidative cyanation using a model reactant, benzyl alcohol. Figure S12 in the Supporting Information shows data characterizing benzyl alcohol conversion as a function of time as the reaction was catalyzed by 0.1Ru/MnO_2-*r*, MnO_2-*r*, and A-MnO_2. MnO_2-*r* gave almost full conversion of benzyl alcohol after 90 min under our conditions, showing that it is more active than A-MnO_2 (17% conversion after 90 min), consistent with the known high activity of nanorod-MnO_2.[35,36] Significantly, addition of 0.1 wt% Ru to this catalyst led to complete conversion after just 45 min, giving a measure of the promotion effect of the Ru sites on the catalytic performance. Moreover, the 0.1Ru/MnO_2-*r* and

MnO_2-*r* was found to be characterized by apparent activation energy (E_a) values of 29.2 and 40.1 kJ/mol, respectively (Figure S13 in the Supporting Information). The marked lowering of E_a upon addition of Ru to the catalyst further demonstrates the benefit of the Ru. Also significant, catalysts consisting of of 0.1 wt% Ru on silica, carbon, or alumina (Table S3 in the Supporting Information) were characterized by undetectable benzyl alcohol conversion or nitrile formation under our conditions (Figure S14 in the Supporting Information), further demonstrating that both the Ru and MnO_2-*r* are necessary for a highly efficient oxidative cyanation catalyst.

It has been reported that benzaldehyde is an intermediate in the oxidative cyanation to synthesize nitriles.[2,8,36,37] This reaction proceeds *via* oxidative dehydrogenation of alcohol to give aldehyde, aldehyde-ammonia condensation to afford imine, and oxidative dehydrogenation to form nitrile (Figure 5a).[2,8,37] As shown by data characterizing the transformation of benzyl alcohol and benzaldehyde under oxidative cyanation conditions, the reaction converting benzaldehyde is generally faster than that converting benzyl alcohol for each catalyst (Figure 5b, Figure S15 in the Supporting Information), a comparison that suggests that the alcohol dehydrogenation (alcohol-to-aldehyde transformation) is the kinetically crucial reaction in the network of the oxidative cyanation process, consistent with the imine dehydrogenation being known as extremely fast.[36-38]

Further insight into the reaction scheme was gained from experiments to determine H/D kinetic isotope effect (KIE). The k_H/k_D value was measured by using benzyl

alcohol ($PhCH_2OH$) and for comparison isotopically labeled benzyl alcohol ($PhCD_2OH$) as substrates, giving the value $k_H/k_D = 6.5$ (determined from the pseudo first-order rate constants $k_H = 5.1 \times 10^{-2}$ min^{-1} and $k_D = 7.9 \times 10^{-3}$ min^{-1}, Figure S16 in the Supporting Information). Such a high k_H/k_D value suggests that the cleavage of the C–H bond at the benzylic position is rate-determining, with the dehydrogenation of OH species occurring facilly.[39-42]

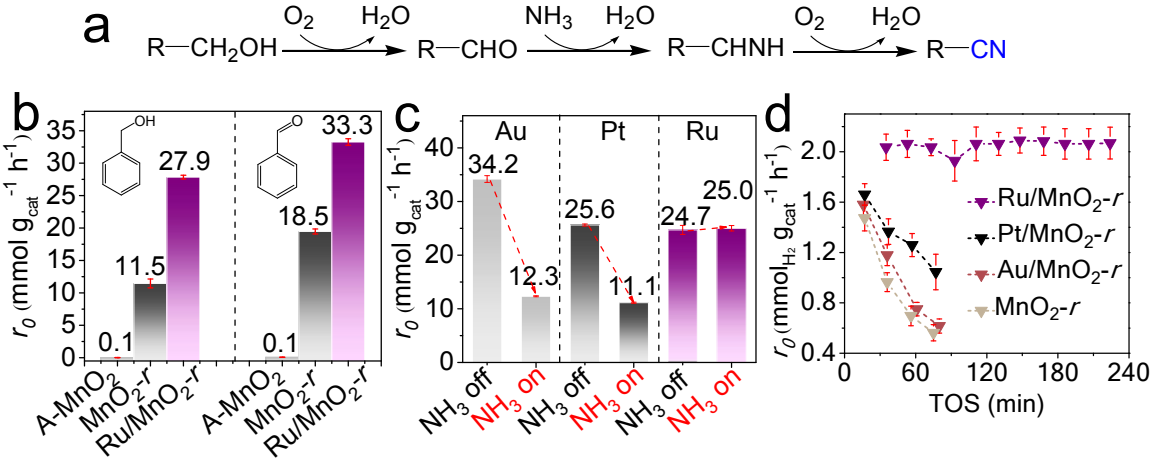

Figure 5. (a) Proposed sequence of reactions in the oxidative cyanation of alcohols to nitriles. (b) Average reaction rate (r_0) in the conversion of benzyl alcohol and benzaldehyde catalyzed by A-MnO_2, MnO_2-*r*, and 0.1Ru/MnO_2-*r*. (c) Average reaction rate (r_0) in the conversion of benzyl alcohol catalyzed by Au/MnO_2-*r*, Pt/MnO_2-*r*, and Ru/MnO_2-*r*. Reaction conditions for (b) and (c): 0.4 mmol of substrate, 4 mL of *t*-amyl alcohol solvent, 100 μL of aqueous NH_3 (28–30 wt%), 1.5 MPa of oxygen, 75 °C. The conversions were controlled to be in the range of 0–20% for calculating the average reaction rates (which, in the limit of zero conversion, approach true reaction rates). (d) Average H_2 production rate in the dehydrogenation of methanol with ammonia in the fed gas with various catalysts. Reaction conditions: 100 mg of catalyst, 300 °C, methanol feed rate, 1.2 mL/h; 1% NH_3/N_2 flow rate of 10 sccm.

Recognizing that supported Au and Pt catalysts are efficient for oxidative

dehydrogenation of alcohols,[39-42] we compared the catalytic activities in oxidative dehydrogenation of benzyl alcohol with and without ammonia, with the catalysts being Au/MnO_2-*r*, Pt/MnO_2-*r*, Ru/MnO_2-*r*, and some others (Figures 5c, Figures S14, S17, and S18, Tables S6 and S7 in the Supporting Information). Notably, the Au/MnO_2-*r*, Pt/MnO_2-*r*, and MnO_2-*r* are characterized by average reaction rates of 34.2, 25.6, and 18.6 mmol g_{cat}^{-1} h^{-1} in the absence of ammonia, and the reaction on catalysts with Au and Pt was found to be faster than that on Ru/MnO_2-*r* (average reaction rate, 24.7 mmol g_{cat}^{-1} h^{-1}). After introduction of ammonia into the reacting liquid, the Au/MnO_2-*r*, Pt/MnO_2-*r*, and MnO_2-*r* catalysts were characterized by significantly reduced average rates (12.3, 11.1, and 11.5 mmol g_{cat}^{-1} h^{-1}), whereas the Ru/MnO_2-*r* catalyst still gave a high benzyl alcohol oxidative dehydrogenation average rate of 25.0 mmol g_{cat}^{-1} h^{-1}. This comparison suggests the possibility of strong inhibition of the Au and Pt by coordination of ammonia.[43,44]

Comparisons of the various catalysts for dehydrogenation in the presence of ammonia were performed with methanol reactant, which was chosen because methanol is the simplest alcohol and usually employed for evaluations of the dehydrogenation activity.[45,46] In these tests without oxygen in the feed, deep dehydrogenation occurred to form CO and H_2 as the products, and the toxic products (e.g., HCN) did not. With regard to a comparison of the dehydrogenation activities, the data show clearly that the Ru/MnO_2-*r* catalyst is much more active than the others, including Au/MnO_2-*r*, Pt/MnO_2-*r*, and MnO_2-*r* (Figure 5d). We stress that the Ru/MnO_2-*r* is stable for hydrogen production in the presence of ammonia, demonstrating its superior ammonia-

resistance. This result is in good agreement with the well-known function of Ru catalysts, which are widely used in ammonia synthesis.[47,48]

Furthermore, the approximate experimental reaction orders, that is, the dependence of average reaction rate on the concentrations of NH_3 and alcohol in the reaction catalyzed by Ru/MnO_2-*r* and MnO_2-*r*, also indicate the enhanced ammonia-resistance of Ru/MnO_2-*r* (Figure S19 in the Supporting Information). These results might help to explain the superior catalytic performance of Ru/MnO_2-*r* in the oxidative cyanation of alcohols, which is strongly correlated with its high activity for oxidative dehydrogenation of alcohols in the presence of ammonia.

3.6. DFT Simulations. To help elucidate the role of Ru in the catalysis, we did DFT simulations by employing single-site Ru anchored on the surface of an α-MnO_2 nanorod as a model of the Ru/MnO_2-*r* catalyst (Figures S20 and S21 in the Supporting Information). For comparison, in the simulations we replaced Ru with Au and, alternatively, with Pt (Figure S22 in the Supporting Information). Figure 6 shows adsorption energies (E_{ads}) of various substrate molecules and energy profiles characterizing the steps during benzyl alcohol dehydrogenation on the Au-, Pt-, and Ru-decorated α-MnO_2 nanorod, along with the proposed steps for $PhCH_2OH$ dehydrogenation on the Ru/MnO_2-*r* catalyst with pre-adsorbed NH_3. Multiple structures and reaction pathways were considered, and only the most energetically favorable ones are shown here.

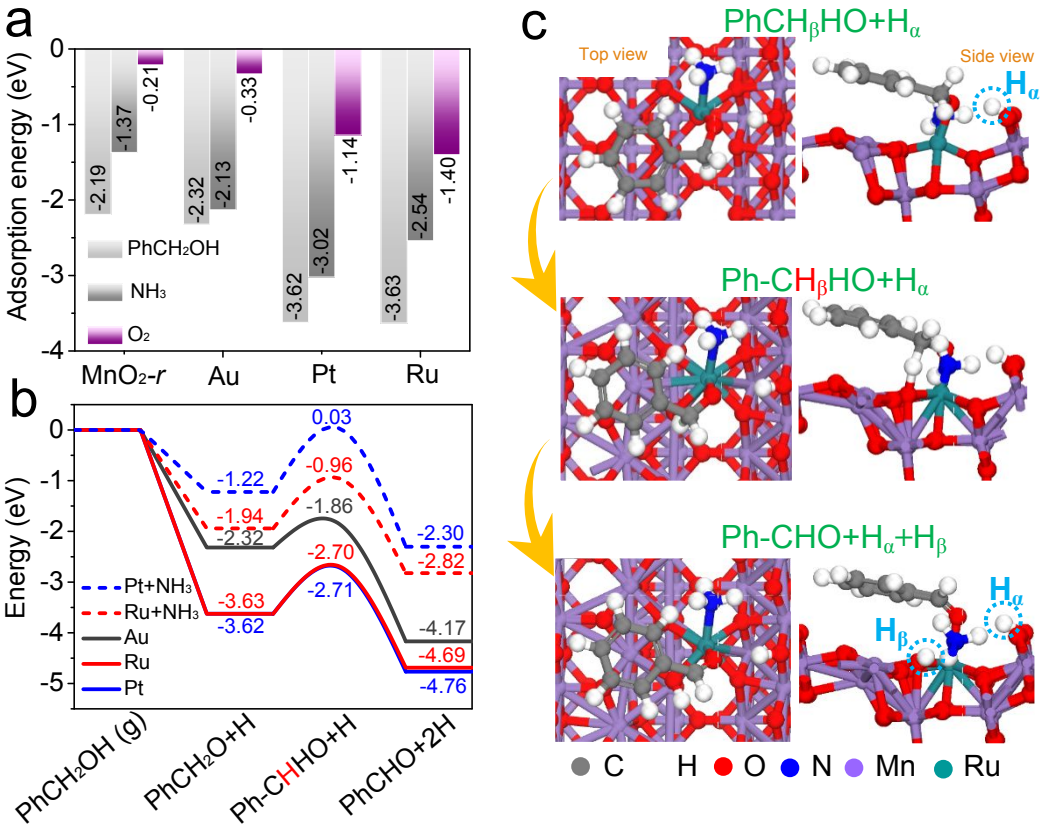

Figure 6. (a) Adsorption energies of $PhCH_2OH$, NH_3, and O_2 on MnO_2-*r*, Au/MnO_2-*r*, Pt/MnO_2-*r*, and Ru/MnO_2-*r*. (b) Energy profiles for $PhCH_2OH$ dehydrogenation on Au/MnO_2-*r*, Pt/MnO_2-*r*, Ru/MnO_2-*r*, Pt+NH_3/MnO_2-*r*, and Ru+NH_3/MnO_2-*r*. (c) The proposed $PhCH_2OH$ dehydrogenation steps on Ru/MnO_2-*r* catalyst with pre-adsorbed NH_3 (Ru+NH_3/MnO_2-*r*).

The results show that benzyl alcohol can be efficiently adsorbed on MnO_2-*r*, with an E_{ads} of -2.19 eV. With Au, Pt, or Ru sites on the MnO_2-*r*, the benzyl alcohol tends to adsorb on these sites, as confirmed by the E_{ads} values of -2.32, -3.62, and -3.63 eV, respectively (Figure 6a). Furthermore, these metal sites also enhance the oxygen adsorption on the catalyst relative to what occurs on bare MnO_2-*r*, particularly for the Pt- and Ru-containing catalysts, with E_{ads} values of -1.14 and -1.40 eV, respectively. Thus, these sites should benefit the oxidation reactions.[40,49]

To elucidate the differences between Au, Pt, and Ru sites, we performed

calculations to determine the energetics of the dehydrogenation process converting benzyl alcohol to benzaldehyde. When a benzyl alcohol molecule adsorbs on one of the metal atoms (Au, Pt, or Ru), the hydrogen atom of the hydroxyl group (denoted as H_α, Figures S23-25 in the Supporting Information) transfers to a nearby surface oxygen atom (denoted as O_α) to form an adsorbed $H_\alpha O_\alpha$* species, resulting the benzyl alkoxide ($PhCH_2O$-) intermediate on the noble metal. This step is regarded as the most favorable first step in alcohol oxidation, consistent with the reported results.[40-42,50] Thereafter, the adsorbed benzyl alkoxide ($PhCH_2O$-) undergoes the second deprotonation process, whereby the C–H bond at the benzylic position undergoes dissociation, giving the hydrogen atom (denoted as H_β) that adsorbs at the adjacent oxygen atom on the support (denoted as O_β) to produce the adsorbed benzaldehyde (Figures S23-25 in the Supporting Information).[40-42,50]

In the C–H cleavage step, the Au-, Pt-, and Ru-containing catalysts are characterized by the energy barriers 0.46, 0.91, and 0.93 eV, respectively (Figure 6b, Table S8 in the Supporting Information). This result suggests that the C–H cleavage is the kinetically crucial step in the benzyl alcohol dehydrogenation, which is also confirmed experimentally by the KIE results (Figure S16 in the Supporting Information). The lower energy barrier for reaction on Au- than on Ru- and Pt-containing catalysts is in agreement with the higher activity of Au/MnO_2-*r* in the benzyl alcohol dehydrogenation indicated by the results of the kinetics experiments (Figure 5c).

The calculations show that when ammonia is introduced onto the catalyst surface, its adsorption by interaction of the lone pair electrons of the N atom is favored on the metal sites rather than on the MnO_2-*r* matrix (Figure 6a and Figure S26 in the Supporting Information).[29,43,51] Thus, there is a competition between benzyl alcohol and ammonia for adsorption on Au sites, as is made evident by the comparable E_{ads} values characterizing ammonia and benzyl alcohol molecules (-2.32 and -2.13 eV, respectively). The calculations, after structure optimization, show that desorption of benzyl alcohol from the catalyst surface takes place when benzyl alcohol and ammonia are co-adsorbed, and so the alcohol dehydrogenation on the Au sites is hindered (Figure 6a and Figure S27 in the Supporting Information).[43]

In contrast, the Pt- and Ru-containing catalysts are characterized by stronger adsorption of the alcohol than of ammonia, but their energy barriers for the cleavage of the C–H bond in these substrates are quite different. For example, the energy barrier for the C–H bond cleavage characterizing ammonia on the Pt-containing catalyst is 1.25 eV, which is much higher than that when ammonia is absent (0.91 eV, Figure 6b, and Table S9 in the Supporting Information). The increased energy barrier for the C–H bond cleavage in the presence of ammonia is ascribed to the lack of availability of the reactive oxygen species for C–H bond cleavage, because the NH_3 molecule occupies the site for this neighboring oxygen species on the Pt atom (Figure S28 in the Supporting Information).

To summarize: These results confirm the strong inhibition by ammonia in the

catalytic dehydrogenation on Au- and Pt-containing catalysts—inhibition caused by hindering the alcohol adsorption on Au and enhancing the C–H cleavage barrier, on Pt.

In contast, and of central importance to the work reported here, the Ru-containing catalyst with coordinated ammonia is characterized by an energy barrier for C–H bond cleavage of 0.98 eV, a value that is close to the value characterizing the ammonia-free case (0.93 eV, Figure 6b, Table S9 in the Supporting Information).

We stress that the MnO_2-*r* without Ru also shows activity for the reaction, which motivated our further calculations characterizing the bare MnO_2-*r* surface. The energy barrier for C–H bond cleavage was found to be 0.45 eV with ammonia present, which is even lower than that of 0.98 eV characterizing that on the Ru on the Ru/MnO_2-*r* surface. After the dehydrogenation step, the hydrogen atoms can reduce the reactive oxygen to form water and oxygen vacancies (O_{vac}) on the MnO_2-*r* surface. A complete reaction cycle requires the regeneration of the reactive oxygen species preceding the adsorption and dissociation of molecular oxygen. The calculated adsorption energy of molecular oxygen over reduced MnO_2-*r* (one oxygen vacancy near an Mn site, Mn-O_{vac}) is -0.45 eV (Figure S29a in the Supporting Information) and the corresponding activation barrier of oxygen dissociation is 2.35 eV (Figures S29b and S29c in the Supporting Information). The high dissociation energy barrier of oxygen suggests that the oxygen regeneration is unfavourable in the continuous dehydrogenation of more alcohol molecules on the MnO_2-*r*.

Further calculations demonstrated that more neighboring oxygen vacancies could

lower the energy barrier. For example, the calculations show that the existence of two neighboring oxygen vacancies around an Mn site leads to an oxygen dissociation barrier of 1.76 eV (Figures S29b and S29d in the Supporting Information)— but the value is still high.

It should be noted here that, under the practical reaction conditions, ammonia might be competing with molecular oxygen at the vacancy sites over catalyst surface. As shown in Figure S30 in the Supporting Information, the ammonia favors occupancy of the Mn-O_{vac} site to suppress the oxygen adsorption, as is shown by the enhanced adsorption energy (Figure S29a in the Supporting Information and Figure 6a). Significantly, the Ru sites on MnO_2-*r* efficiently decrease the oxygen dissociation barrier, with a value of 0.56 eV on the oxygen vacancy close a Ru atom (Figures S31 and S32, Table S10 in the Supporting Information), which is much lower than what we calculated for reaction on MnO_2-*r*: values in the range of 1.76–2.35 eV. Even with the presence of ammonia, the oxygen dissociation barrier still appeared at 0.69 eV on the Ru/MnO_2-*r* (Figure S33 in the Supporting Information). These values are also much smaller than that characterizing the inert oxide-supported Ru (e.g., Ru/Al_2O_3 in Figures S34 and S35 in the Supporting Information).

In summary, on the basis of these results characterizing substrate adsorption, C–H cleavage, and regeneration of the reactive oxygen surface species, we suggest that the Ru/MnO_2-*r* catalyst appears to be optimal for continuous $PhCH_2OH$ dehydrogenation in the presence of ammonia (Figure 6c), which might explain the high

activity of the Ru/MnO_2-*r* catalyst for oxidative cyanation.

4. CONCLUSIONS

The experimental and computational results presented here show that 0.1Ru/MnO_2-*r* is an active, selective, and stable catalyst for the oxidative cyanation of various alcohols to give the corresponding nitriles. Previous investigations showed that alumina-supported $Ru(OH)_3$ catalyzes the oxidative cyanation when the catalyst Ru content is high, and such catalysts with low Ru contents were regrded as inactive. Now we have found that MnO_2-*r* containing atomically dispersed Ru with a loading of only 0.1 wt% is highly active for this reaction. The Ru is a promoter; this role has not been reported before. Both the Ru–O–MnO_x and MnO_2 regions could catalyze the oxidative cyanation, while the former providing for a much higher activity than characterizes just MnO_2. The low Ru content is advantageous in terms of catalyst cost, with the efficiency of use of this metal being superior to those of reported Ru-containing catalysts. Furthermore, the 0.1Ru/MnO_2-*r* catalyst is simple enough in structure to constitutes a good foundation for computational and experimental investigations of oxidative cyanations. Specifically, the catalyst lends itself to investigation of the various roles of ammonia in the reaction, including it role as an inhibitor, which is crucial for any practical application. Moreover, the 0.1Ru/MnO_2-*r* also provides new insights into single-site catalysis, extending the field to include manganese oxide as a support and complementing the extensive literature of such catalysts supported on ceria,[27,40] ferric

oxide,[28,31] and titania.[52]

In summary, we have develped a manganese nanorod-supported single-site Ru catalyst for the nitrile synthesis from oxidative cyanation of a wide range of alcohols. The experimental and theoretical results summarized here demonstrate that the single-site Ru species enhance the ammonia-resistance of the catalyst, acclerate the C–H bond cleavage and molecular oxygen activation. This work suggests opportunities for the *proof-of-concept* design of more efficient catalysts for oxidative cyanations.

AUTHOR INFORMATION

Corresponding Author

Email: liangwang@zju.edu.cn (L.W.)

Email: yangbo1@shanghaitech.edu.cn (B.Y.)

Email: fsxiao@zju.edu.cn (F.-S.X.)

Author Contributions

H. Wang, D. Xu, and E. Guan contributed equally.

Notes

The authors declare no competing financial interest.

ASSOCIATED CONTENT

Supporting Information

Additional characterization data, XRD patterns; TEM images; HAADF-STEM images, elemental maps; EXAFS spectra; XP spectra, catalytic and kinetic data, DFT simulations. The Supporting Information is available free of charge on the ACS Publications website.

ACKNOWLEDGMENTS

This work was supported by the National Key Research and Development Program of China (2018YFB0604801), the National Natural Science Foundation of China (21822203 and 91634201), the Natural Science Foundation of Zhejiang Province (LR18B030002), and the U.S. Department of Energy (DOE), Office of Science, Basic Energy Sciences (BES) grant DE-FG02-04ER15513, and the Fundamental Research Funds for the Central Universities. We ackowledge beam time at the 8-ID (ISS) beamline of the NSLS-II, a DOE Office of Science User Facility operated for the Office of Science by Brookhaven National Laboratory under Contract No. DE-AC02-98CH10886. We thank Prof. Wei Zhang and Fang Chen for kind help in the TEM characterization.

REFERENCES

(1) Hodgson, H. H. The Sandmeyer Reaction. *Chem. Rev*. 1947, *40*, 251-277.

(2) Jagadeesh R. V.; Junge H.; Beller, M. Green Synthesis of Nitriles Using Non-Noble Metal Oxides-Based Nanocatalysts. *Nat. Commun.* **2014**, *5*, 4123.

(3) Wang, L.; Wang, G.; Zhang, J.; Bian, C.; Meng, X.; Xiao, F.-S. Controllable Cyanation of Carbon-Hydrogen Bonds by Zeolite Crystals over Manganese Oxide Catalyst. *Nat. Commun.* **2017**, *8*, 15240.

(4) Jia, X.; Ma, J.; Xia, F.; Xu, Y.; Gao, J.; Xu, J. Carboxylic Acid-Modified Metal Oxide Catalyst for Selectivity-Tunable Aerobic Ammoxidation. *Nat. Commun.* **2018**, *9*, 933.

(5) Anbarasan, P.; Schareina, T.; Beller, M. Recent Developments and Perspectives in Palladium-Catalyzed Cyanation of Aryl Halides: Synthesis of Benzonitriles. *Chem. Soc. Rev.* **2011**, *40*, 5049-5067.

(6) Varma, R. S.; Naicker, K. P. The Urea−Hydrogen Peroxide Complex: Solid-State Oxidative Protocols for Hydroxylated Aldehydes and Ketones (Dakin Reaction), Nitriles, Sulfides, and Nitrogen Heterocycles. *Org. Lett.* **1999**, *1*, 189-191.

(7) Varma, R. S.; Naicker, K. P. Hydroxylamine on Clay: a Direct Synthesis of Nitriles from Aromatic Aldehydes Using Microwaves Under Solvent-Free Conditions. *Molecules Online* **1998**, *2*, 94-96.

(8) Oishi, T.; Yamaguchi, K.; Mizuno, N. Catalytic Oxidative Synthesis of Nitriles Directly from Primary Alcohols and Ammonia. *Angew. Chem. Int. Ed.* **2009**, *48*, 6286-6288.

(9) Martin, A.; Kalevaru, N. V.; Lücke, B.; Sans, J. Eco-Friendly Synthesis of *p*-Nitrobenzonitrile by Heterogeneously Catalysed Gas Phase Ammoxidation. *Green Chem.* **2002**, *4*, 481-485.

(10) Dornan, L. M.; Cao, Q.; Flanagan, J. C.; Crawford, J. J.; Cook, M. J.; Muldoon, M. J. Copper/TEMPO Catalysed Synthesis of Nitriles from Aldehydes or Alcohols Using Aqueous Ammonia and with Air as the Oxidant. *Chem. Commun.* **2013**, *49*, 6030-6032.

(11) Yin, W.; Wang, C.; Huang, Y. Highly Practical Synthesis of Nitriles and Heterocycles from Alcohols Under Mild Conditions by Aerobic Double Dehydrogenative Catalysis. *Org. Lett.* **2013**, *15*, 1850-1853

(12) Shang, S.; Wang, L.; Dai, W.; Chen, B.; Lv, Y.; Gao, S. High Catalytic Activity of Mesoporous Co-N/C Catalysts for Aerobic Oxidative Synthesis of Nitriles *Catal. Sci. Technol.* **2016**, *6*, 5746-5753.

(13) Ishida, T.; Watanabe, H.; Takei, T.; Hamasaki, A.; Tokunaga, M.; Haruta, M. Metal Oxide-Catalyzed Ammoxidation of Alcohols to Nitriles and Promotion Effect of Gold Nanoparticles for One-Pot Amide Synthesis. *Appl. Catal. A* **2012**, *425*, 85-90.

(14) Preger, Y.; Root, T. W.; Stahl, S. S. Platinum-Based Heterogeneous Catalysts for Nitrile Synthesis via Aerobic Oxidative Coupling of Alcohols and Ammonia. *ACS Omega*, **2018**, *3*, 6091-6096.

(15) Wang, Y.; Yamaguchi, K.; Mizuno, N. Manganese Oxide Promoted Liquid-Phase Aerobic Oxidative Amidation of Methylarenes to Monoamides Using Ammonia Surrogates. *Angew. Chem. Int. Ed.* **2012**, *51*, 7250-7253.

(16) Yamaguchi, K.; Kobayashi, H.; Wang, Y.; Oishi, T.; Ogasawara, Y.; Mizuno, N. Green Oxidative Synthesis of Primary Amides from Primary Alcohols or Aldehydes Catalyzed by a Cryptomelane-Type Manganese Oxide-Based Octahedral Molecular Sieve, OMS-2. *Catal. Sci. Technol*. **2013**, *3*, 318-327.

(17) Newville, M. EXAFS Analysis Using *FEFF* and *FEFFIT*. *J Synchrotron Rad.* **2001**, *8*, 96-100.

(18) Bolzan, A. A.; Fong, C.; Kennedy, B. J.; Howard, C. J. Structural Studies of Rutile-Type Metal Dioxides. *Acta Cryst.* **1997**, *53*, 373-380.

(19) Wang, L.; Zhu, Y.; Wang, J.-Q.; Liu, F.; Huang, J.; Meng, X.; Basset, J.-M.; Han, Y.; Xiao, F.-S. Two-Dimensional Gold Nanostructures with High Activity for Selective Oxidation of Carbon-Hydrogen Bonds. *Nat. Commun.* **2015**, *6*, 6957.

(20) Dugal, M.; Sankar, G.; Raja, R.; Thomas, J. M. Designing a Heterogeneous Catalyst for the Production of Adipic Acid by Aerial Oxidation of Cyclohexane. *Angew. Chem. Int. Ed.* **2000**, *39*, 2310-2313.

(21) Kresse, G.; Furthmuller, J. Efficient Iterative Schemes for Ab Initio Total-Energy

Calculations Using a Plane-Wave Basis Set. *Phys. Rev. B* **1996**, *54*, 11169-11186.

(22) Kresse, G.; Joubert, D. From Ultrasoft Pseudopotentials to the Projector Augmented-Wave Method. *Phys. Rev. B* **1999**, *59*, 1758-1775.

(23) Grimme, S.; Antony, J.; Ehrlich, S.; Krieg, H. A Consistent and Accurate Ab Initio Parametrization of Density Functional Dispersion Correction (DFT-D) for the 94 Elements H-Pu. *J. Chem. Phys.* **2010**, *132*, 154104.

(24) Tompsett, D.; Parker, S.; Islam, M. S. Surface Properties of α-MnO_2: Relevance to Catalytic and Supercapacitor Behaviour. *J. Mater. Chem. A* **2014**, *2*, 15509-15518.

(25) Johnson, C. S.; Dees, D. W.; Mansuetto, M. F.; Thackeray, M. M.; Vissers, D. R.; Argyriou, D.; Loong, C. K.; Christensen, L. Structural and Electrochemical Studies of α-Manganese Dioxide (α-MnO_2). *J. Power Sources* **1997**, *68*, 570-577.

(26) Sueoka, S.; Mitsudome, T.; Mizugaki, T.; Jitsukawa, K.; Kaneda, K. Supported Monomeric Vanadium Catalyst for Dehydration of Amides to Form Nitriles. *Chem. Commun.* **2010**, *46*, 8243-8245.

(27) Nie, L.; Mei, D.; Xiong, H.; Peng, B.; Ren, Z.; Hernandez, X. I. P.; DeLaRiva, A.; Wang, M.; Engelhard, M. H.; Kovarik, L.; Datye, A. K.; Wang, Y. Activation of Surface Lattice Oxygen in Single-Atom Pt/CeO_2 for Low-Temperature CO Oxidation. *Science* **2017**, *358*, 1419-1423.

(28) Qiao, B.; Wang, A.; Yang, X.; Allard, L. F.; Jiang, Z.; Cui, Y.; Liu, J.; Li, J.; Zhang, T. Single-Atom Catalysis of CO Oxidation Using Pt_1/FeO_x. *Nat. Chem.* **2011**, *3*, 634-641.

(29) Deng, W.; Wang, Y.; Zhang, S.; Guptaa, K. M.; Hülsey, M. J.; Asakura, H.; Liu, L.; Han, Y.; Karp, E. M.; Beckham, G. T.; Dyson, P. J.; Jiang, J.; Tanaka, T.; Wang, Y.; Yan, N. Catalytic Amino Acid Production from Biomass-Derived Intermediates. *Proc. Natl. Acad. Sci. USA* **2018**, *115*, 5093-5098.

(30) Komanoya, T.; Kinemura, T.; Kita, Y.; Kamata, K.; Hara, M. Electronic Effect of Ruthenium Nanoparticles on Efficient Reductive Amination of Carbonyl Compounds. *J. Am. Chem. Soc.* **2017**, *139*, 11493-11499.

(31) Wei, H.; Liu, X.; Wang, A.; Zhang, L.; Qiao, B.; Yang, X.; Huang, Y.; Miao, S.; Liu, J.; Zhang, T. FeO_x-Supported Platinum Single-Atom and Pseudo-Single-Atom

Catalysts for Chemoselective Hydrogenation of Functionalized Nitroarenes. *Nat. Commun.* **2014**, *5*, 5634.

(32) Chen, Y.; Ji, S.; Sun, W.; Chen, W.; Dong, J.; Wen, J.; Zhang, J.; Li, Z.; Zheng, L.; Chen, C.; Peng, Q.; Wang, D.; Li, Y. Discovering Partially Charged Single-Atom Pt for Enhanced Anti-Markovnikov Alkene Hydrosilylation. *J. Am. Chem. Soc.* **2018**, *140*, 7407-7410.

(33) Aitbekova, A.; Wu, L.; Wrasman, C. J.; Boubnov, A.; Hoffman, A. S.; Goodman, E. D.; Bare, S. R.; Cargnello, M. Low-Temperature Restructuring of CeO_2-Supported Ru Nanoparticles Determines Selectivity in CO_2 Catalytic Reduction. *J. Am. Chem. Soc.* **2018**, *140*, 13736-13745.

(34) Mori, K.; Taga, T.; Yamashita, H. Isolated Single-Atomic Ru Catalyst Bound on a Layered Double Hydroxide for Hydrogenation of CO_2 to Formic Acid. *ACS Catal.* **2017**, *7*, 3147-3151.

(35) Gu, D.; Tseng, J.-C.; Weidenthaler, C.; Bongard, H.-J.; Spliethoff, B.; Schmidt, W.; Soulimani, F.; Weckhuysen, B. M.; Schüth, F. Gold on Different Manganese Oxides: Ultra-Low-Temperature CO Oxidation over Colloidal Gold Supported on Bulk-MnO_2 Nanomaterials. *J. Am. Chem. Soc.* **2016**, *138*, 9572-9580.

(36) Wang, H.; Wang, L.; Wang, S.; Dong, X.; Zhang, J.; Xiao, F.-S. Aerobic Activation of C-H Bond in Amines over a Nanorod Manganese Oxide Catalyst. *ChemCatChem* **2019**, *11*, 401-406.

(37) Yamaguchi, K.; Mizuno, N. Scope, Kinetics, and Mechanistic Aspects of Aerobic Oxidations Catalyzed by Ruthenium Supported on Alumina. *Chem. Eur. J.* **2003**, *9*, 4353-4361.

(38) Yamaguchi, K.; Mizuno, N. Efficient Heterogeneous Aerobic Oxidation of Amines by a Supported Ruthenium Catalyst. *Angew. Chem. Int. Ed.* **2003**, *42*, 1480-1483.

(39) Wang, F.; Ueda, W.; Xu, J. Detection and Measurement of Surface Electron Transfer on Reduced Molybdenum Oxides (MoO_x) and Catalytic Activities of Au/MoO_x. *Angew. Chem. Int. Ed.* **2012**, *51*, 3883-3887.

(40) Li, T.; Liu, F.; Tang, Y.; Li, L.; Miao, S.; Su, Y.; Zhang, J.; Huang, J.; Sun, H.; Haruta, M.; Wang, A.; Qiao, B.; Li, J.; Zhang, T. Maximizing the Number of

Interfacial Sites in Single-Atom Catalysts for The Highly Selective, Solvent-Free Oxidation of Primary Alcohols. *Angew. Chem. Int. Ed.* **2018**, *57,* 7795-7799.

(41) Zhu, X.; Guo, Q.; Sun, Y.; Chen, S.; Wang, J.-Q.; Wu, M.; Fu, W.; Tang, Y.; Duan, X.; Chen, D.; Wan, Y. Optimising Surface d Charge of AuPd Nanoalloy Catalysts for Enhanced Catalytic Activity. *Nat. Commun.* **2019**, *10*, 1428.

(42) Zhao, G.; Yang, F.; Chen, Z.; Liu, Q.; Ji, Y.; Zhang, Y.; Niu, Z.; Mao, J.; Bao, X.; Hu, P.; Li, Y. Metal/Oxide Interfacial Effects on the Selective Oxidation of Primary Alcohols. *Nat. Commun.* **2017**, *8*, 14039.

(43) Yongprapat, S.; Therdthianwong, A.; Therdthianwong, S. Effects of NH_3 and Tertiary Ammoniums on Au/C Catalyst in Glycerol Electrooxidation in Alkaline Media. *J. Appl. Electrochem.* **2015**, *45*, 487-494.

(44) Pendyala, V. R. R.; Shafer, W. D.; Jacobs, G.; Martinelli, M.; Sparks, D. E.; Davis, B. H. Fischer-Tropsch Synthesis: Effect of Ammonia on Product Selectivities for a Pt Promoted Co/Alumina Catalyst. *RSC Adv.* **2017**, *7*, 7793-7800.

(45) Greeley, J.; Mavrikakis, M. A First-Principles Study of Methanol Decomposition on Pt(111). *J. Am. Chem. Soc.* **2002**, *124*, 7193-7201.

(46) Ou, L. Theoretical Insights into the Effect of Solvation and Sublayer Ru on Pt-Catalytic CH_3OH Oxidation Mechanisms in the Aqueous Phase. *J. Phys. Chem. C* **2018**, *122*, 14554-14565.

(47) Honkala, K.; Hellman, A.; Remediakis, I. N.; Logadottir, A.; Carlsson, A.; Dahl, S.; Christensen, C. H.; Nørskov, J. K. Ammonia Synthesis from First-Principles Calculations. *Science* **2005**, *307*, 555-558.

(48) Lin, B.; Liu, Y.; Heng, L.; Wang, X.; Ni, J.; Lin, J.; Jiang, L. Morphology Effect of Ceria on the Catalytic Performances of Ru/CeO_2 Catalysts for Ammonia Synthesis. *Ind. Eng. Chem. Res.* **2018**, *57*, 9127-9135.

(49) Enache, D. I.; Edwards, J. K.; Landon, P.; Solsona-Espriu, B.; Carley, A. F.; Herzing, A. A.; Watanabe, M.; Kiely, C. J.; Knight, D. W.; Hutchings, G. J. Solvent-Free Oxidation of Primary Alcohols to Aldehydes Using Au-Pd/TiO_2 Catalysts. *Science* **2006**, *311*, 362-365.

(50) Rodriguez, P.; Kwon, Y.; Koper, M. T. M. The Promoting Effect of Adsorbed Carbon Monoxide on the Oxidation of Alcohols on a Gold Catalyst. *Nat. Chem.* **2012**, *4*, 177-182.

(51) Chitpakdeea, C.; Junkaewa, A.; Maitarad, P.; Shi, L.; Promarak, V.; Kungwan, N.; Namuangruk, S. Understanding the Role of Ru Dopant on Selective Catalytic Reduction of NO with NH_3 over Ru-Doped CeO_2 Catalyst. *Chem. Eng. J.* **2019**, *369*, 124-133.

(52) Liu, P.; Zhao, Y.; Qin, R.; Mo, S.; Chen, G.; Gu, L.; Chevrier, D. M., Zhang, P.; Guo, Q.; Zang, D.; Wu, B.; Fu, G.; Zheng, N. Photochemical Route for Synthesizing Atomically Dispersed Palladium Catalysts. *Science* **2016**, *352*, 797-800.

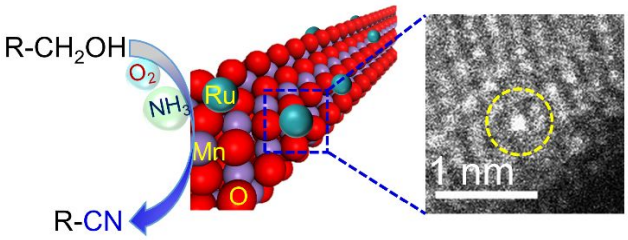

R = aromatic; aliphatic; heterocyclic; allylic